Switchable gas permeability of a polypropylene-liquid crystalline composite film

Received: 22 November 2021 | Revised: 9 December 2021 | Accepted: 9 December 2021

DOI: 10.1002/pol.20210835

RESEARCH ARTICLE

JOURNAL OF POLYMER SCIENCE WILEY

Switchable gas permeability of a polypropylene-liquid crystalline composite film

Simon J. A. Houben[1] | **Joey Kloos**[2] | **Zandrie Borneman**[2] | **Albert P. H. J. Schenning**[1]

[1]Laboratory of Stimuli-responsive Functional Materials and Devices, Department of Chemical Engineering and Chemistry, Eindhoven University of Technology, Eindhoven, Manitoba, The Netherlands

[2]Membrane Materials and Processes, Department of Chemical Engineering and Chemistry, Eindhoven University of Technology, Eindhoven, Manitoba, The Netherlands

Correspondence
Zandrie Borneman, Membrane Materials and Processes, Department of Chemical Engineering and Chemistry, Eindhoven University of Technology, P.O. Box 513, 5600 MB, Eindhoven, The Netherlands.
Email: z.borneman@tue.nl

Albert P. H. J. Schenning, Laboratory of Stimuli-responsive Functional Materials and Devices, Department of Chemical Engineering and Chemistry, Eindhoven University of Technology, P.O. Box 513, 5600 MB The Netherlands.
Email: a.p.h.j.schenning@tue.nl

Abstract

The development of functionalized polyolefins for use as stimuli-responsive commodity polymers has recently received much attention. In this work, a microporous polypropylene (PP) scaffold is used to align and fortify a smectic liquid crystalline network (LCN) which can switch its gas permeability upon pH changes. The LCN is a photopolymerized liquid crystalline mixture of a dimerized benzoic acid derivative monoacrylate and a diacrylate crosslinker. In the hydrogen-bonded state, the composite membrane shows a high-molecular order and a low permeability for He, N_2, and CO_2 gases. By pH switching from the hydrogen-bonded state to the salt form, the molecular order is reduced, and the gas permeability is increased by one order of magnitude. This increase is mainly attributed to a loss in order of the system, increasing the free volume, resulting in an increased diffusibility. By exposing the composite film to basic or acidic environments, reversible switching between low and high gas permeability states is observed, respectively. The physical constraints imposed by the PP scaffold strengthens the membrane while the reversible switching inside the liquid crystalline polymer is maintained. This switching of gas permeation properties is not possible with the fragile freestanding LCN films alone.

KEYWORDS

liquid crystals, polymer barrier coatings, polymer gas membranes, polyolefins, stimuli responsive materials

1 | INTRODUCTION

Advances in polymer technology have led to the fabrication of materials ranging from highly permeable and selective membranes to polymers with low permeabilities for barrier layers.[1–5] These materials are industrially relevant; for instance, the use of gas separation membranes can increase the quality of biogas by removing CO_2,[6,7] and packaging material with high-O_2 barrier properties can increase shelf lives of sealed food products.[4] While developments of both gas permeable and barrier polymers with static properties continue, new opportunities may be found for materials with dynamic, stimuli-responsive permeability properties.

Recent literature has demonstrated dynamic polymers for use as smart coatings,[8,9] soft robotic actuators,[10,11]

switchable membranes,[12–15] and optical sensors[16,17] that respond to stimuli including light,[10,18] temperature,[9] electric and magnetic fields,[19] humidity,[20] and pH.[13,15,21] Often, specialty polymers based on liquid crystals, hydrogels or shape memory polymers are used to create these stimuli responsive materials. Only a few examples exist of materials with changeable gas permeability, and these are limited to light and temperature responsivities.[22–24] Recently, commodity polymers have also been used to fabricate stimuli responsive materials,[14,15,20,25–28] but commodity polymers with switchable gas permeability have not yet been reported.

One promising approach for achieving switchable gas permeable membranes is by using an anisotropic, microporous polyolefin acting as a mechanically strong scaffold for alignment of stimuli responsive liquid crystalline networks (LCNs). An example are humidity responsive actuators based on anisotropic microporous polypropylene (PP)/LCN composites.[20] A similar approach resulted in a nanoporous membrane able to reject small organic dyes.[15] Finally, highly ordered LCNs without dynamic properties have shown suitable for the separation of gasses.[3,29]

This work reports using an anisotropic, PP scaffold with 10–20 nm wide, 100 nm long micropores (Figure 1A), commercially available as Celgard® 2500, to fabricate liquid crystalline polymer composites with switchable gas permeability. A smectic liquid crystalline mixture consisting of hydrogen-bonded LC monoacrylate benzoic acid (I) dimers and smectic diacrylate (II) crosslinkers (the molecular structures are found in Figure 1B) is planarly aligned and polymerized inside the anisotropic porous PP scaffold, resulting in a composite film. By exposing the material to a basic environment, the H-bonds are disrupted, resulting in a polymer salt with a reduced order. Subsequent exposure to an acidic solution restores the H-bonds, and, consequently, some of the order is restored (Figure 1C). This pH response is used to reversibly switch between low and high gas permeability states in the PP-LCN composite film.

2 | RESULTS AND DISCUSSION

For the preparation of the PP-LCN composite film, a smectic liquid crystalline 4:6 ratio mixture of I and II (Figure 1B) was used (described previously).[30–32] During cooling the LC mixture has a smectic A (SmA) phase between 30 and 97 °C. To this LC mixture, a photoinitiator and inhibitor were added. The anisotropic microporous PP scaffold was functionalized with the LCN layer by a transfer method as described in our previous work.[15] Here, however, the LC mixture was not diluted with a solvent, resulting in a complete filling of LC monomers in the microporous scaffold. After filling

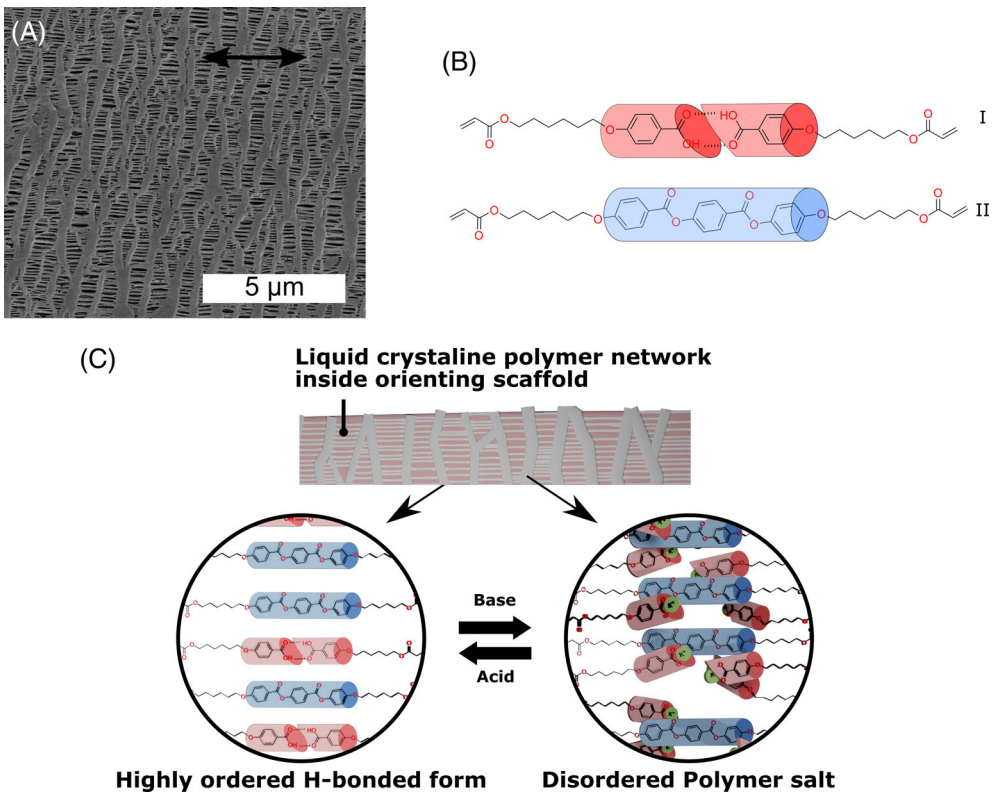

FIGURE 1 (A) Top view scanning electron microscopy (SEM) image of the microporous structure of the anisotropic polypropylene (PP) scaffold (Celgard® 2500) with the fibrillar direction indicated by the black arrow. (B) The molecular structure of the hydrogen-bonded benzoic acid derivative (I) and diacrylate crosslinker (II) used in the liquid crystalline network (LCN). (C) A simplified schematic representation of the PP-LCN composite film. The anisotropic PP is gray. The LCN contains the switchable mesogen (I) depicted in red and the crosslinker (II) in blue. The LCN is aligned parallel to the small fibrils in the porous PP scaffold. Switching in the LCN is possible between hydrogen-bonding and polymer salt state with 0.1 M KOH and HCl

of the scaffold, the LC mixture was first brought into the highly ordered smectic phase and then photopolymerized with UV-light, resulting in a freestanding composite PP-LCN film (see experimental section).[15]

The PP-LCN composite was investigated by scanning electron microscopy (SEM). A cross section of the pristine composite film was made with the cutting direction parallel to both the small fibrils, and LC director (Figure 1A). In Figure 2A, B it is revealed that the 25 μm thick PP scaffold was fully filled with LC, topped by a 2 μm layer of pure LCN.

Wide angle x-ray scattering (WAXS) and medium angle x-ray scattering (MAXS) experiments were performed on the pristine composite film to confirm the alignment and molecular order. In Figure 2C, D the x-ray scattering spectra of the composite film are shown. The formation of a SmA phase with a layer spacing of 3.89 nm is visible with the layers aligned perpendicular to the large fibrils. This indicates that the LC director aligns parallel to the small fibrils (Figure 1A), in accordance with our previous findings.[15]

pH is used as a trigger to induce chemical changes in the network. By exposing the highly ordered nanostructure to a base treatment, the H-bonds are disrupted, resulting in the formation of a polymer salt with a decreased order.[15,32,33] The Fourier transfer infrared (FT-IR) spectrum in Figure 2E confirmed disruption of the H-bonds by the disappearance of the C═O stretch vibration at 1680 cm^{-1} and formation of the potassium carboxylate salt at 1540 cm^{-1}, respectively (illustrated in Figure 2F). After a treatment with an acidic solution, the process was reversed as indicated by the reappearance of the C═O

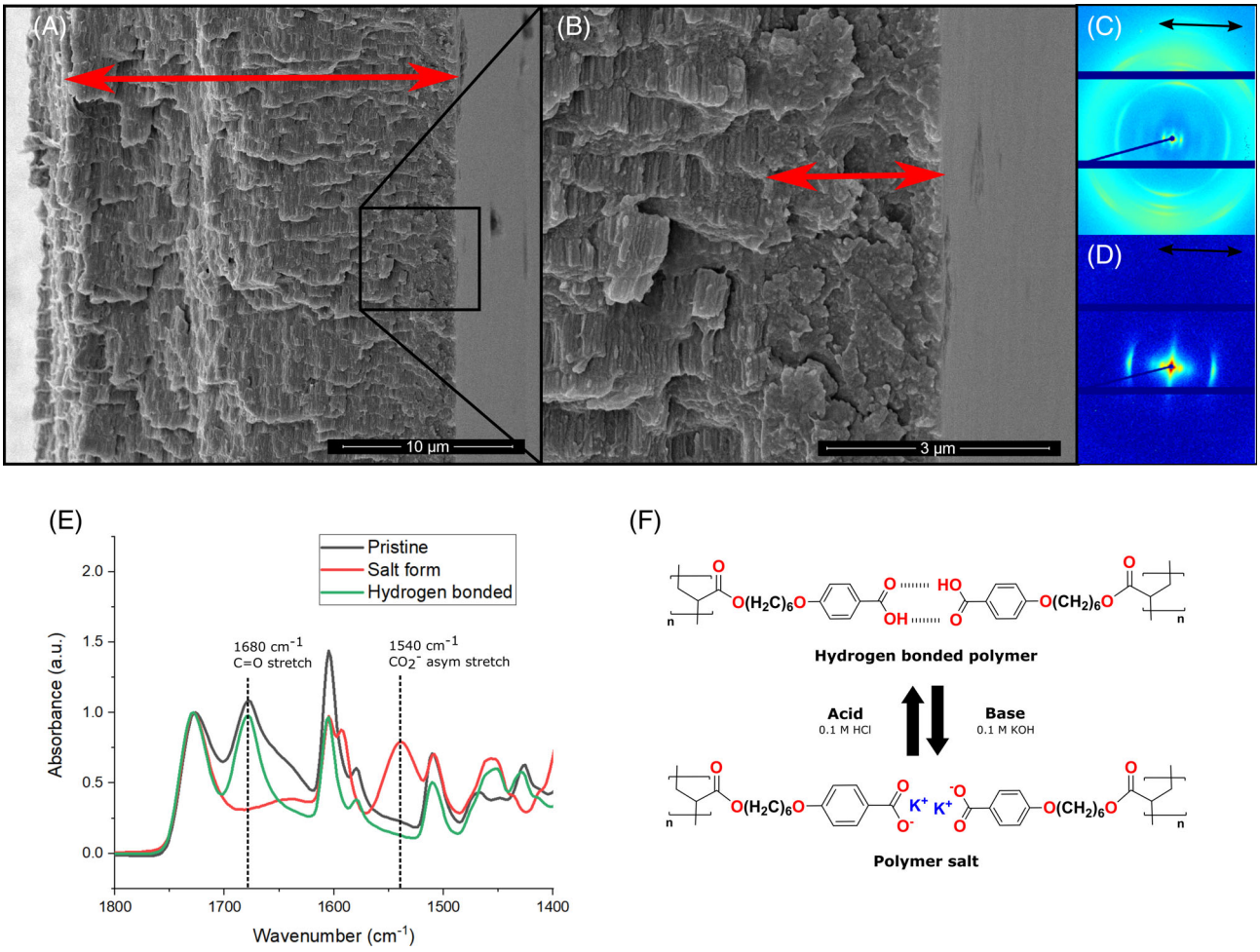

FIGURE 2 Scanning electron microscopy (SEM) image of the cross section (A) of the composite. The red arrows indicate a thickness of 27 μm. An image made at higher magnification (B) showed a top layer of 2 μm of pure liquid crystalline network (LCN) material, indicated with the red arrows, identifiable by the different morphology. Wide angle x-ray scattering (WAXS) (C) and medium angle x-ray scattering (MAXS) (D) of the pristine composite film with black arrows indicating the orientation of the small fibrils. Fourier transfer infrared (FT-IR) spectra (E) of the pristine state (black line), the salt form after alkaline treatment (red line), and the H-bonded state (green line), after acid and basic treatments with (F) respective chemical changes during switching

stretch vibration at 1680 cm^{-1}, typical for the H-bonding between benzoic acid moieties.[30,33,34] Changes of order in the composite film caused by switching between the polymer salt form and H-bonded state were also investigated with WAXS and MAXS experiments. The base treatment resulted in a transition from an ordered 2D layering into a system with reduced order as shown Figure 3A, B. The normally well-defined intermolecular stacking at 0.38 nm appears to become less intense and broader, indicative of order loss. When looking at smaller scattering angles, it is observed that the formerly well-defined SmA spots at 3.9 nm were transformed to a slightly less defined spots with a smaller layer spacing of 3.7 nm accompanied by an isotropic ring. This disorder in the system is caused by the breaking of H-bonds between benzoic acid moieties, so they no longer act as chemical crosslinkers, resulting in softening of the network and giving the benzoic acid moieties the ability to rotate more freely. The remaining 2D order in the system is provided by crosslinker II which keeps the layers together.[31] When exposed to an acidic treatment, the H-bonding is recovered, and the original, aligned morphology was restored, as shown in the WAXS and MAXS spectra in Figure 3C, D. To determine the influence of the scaffold on the making and breaking of the H-bonds, identical alkaline and acidic treatments were performed on a reference sample without fortification by a PP scaffold. After alkaline treatment, a similar isotropic ring is formed as for the composite (see Figure 3E, F) but the scattering intensity is much greater than in the scaffolded sample, indicating an increased loss of order. When returning to the H-bonded state (Figure 3G, H), no restoration of the highly ordered phase is observed: only a faint signal can be seen near 3.9 nm, and the broad band near 0.4 nm originating from the intermolecular stacking no longer seems well-defined. Most likely the differences between the samples with and without the PP scaffold is a result of the physical confinement of the LCN in the micropores. The scaffold probably constrains swelling and forces the material to return to its original order and shape after reformation of the H-bonds.

The switching between the salt form and H-bonded states also resulted in macroscopic shape changes. Whereas the composite film does not visibly change during the switching, the freestanding film does (Figure 4). The freestanding film showed a high degree of deformation in both the salt form and the H-bonded state, as shown in Figure 4D–F. The freestanding film in the salt

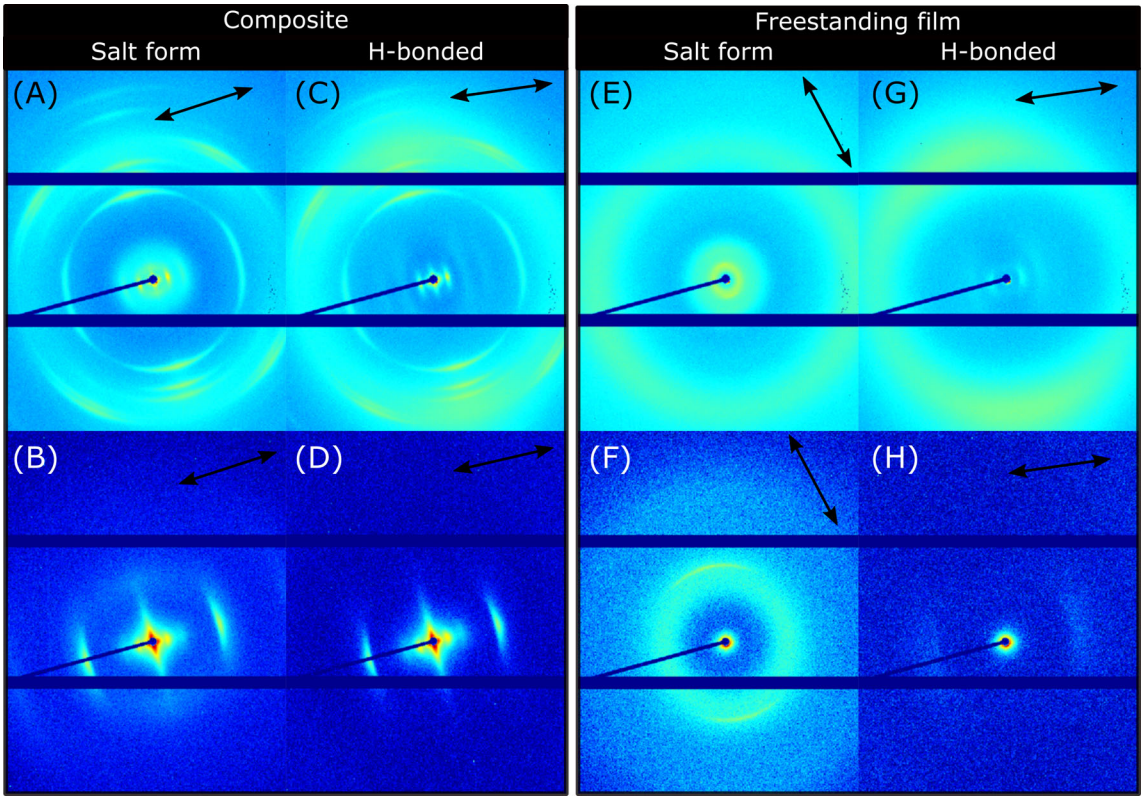

FIGURE 3 Wide angle x-ray scattering (WAXS) (top row) and corresponding medium angle x-ray scattering (MAXS) (bottom row) of the composite film (A–D) and freestanding film (E–H) in the salt form (A, B, E, and F) and in H-bonded form (C, D, G, and H). The alignment directions of the small fibrils of the scaffold are illustrated with the black arrows

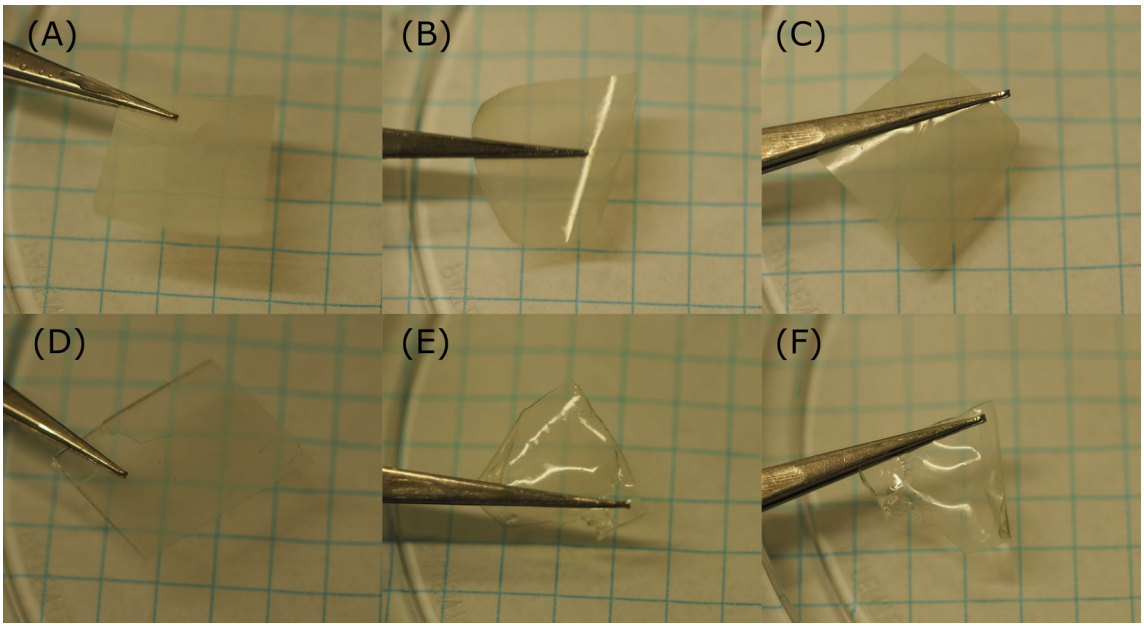

FIGURE 4 Pictures of the composite (A–C) and freestanding films (D-F) in the pristine state (left), polymer salt form (middle) and H-bonded state (right) with a 0.5 mm grid paper as background

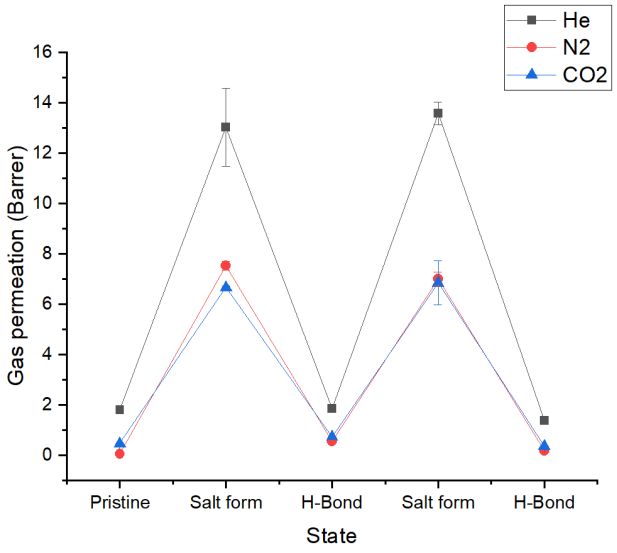

FIGURE 5 Single-gas permeation experiments with the composite film switching between the salt form and the hydrogen-bonded states

form was rather flexible, but both the salt form and the H-bonded form the film were highly susceptible to damage upon bending. These observations indicate the importance of a scaffold to help prevents damage from mechanical deformation and preserve the shape of the pH responsive LCNs.[20]

The gas permeability of the membrane was tested by single-gas (He, N_2, and CO_2) permeation experiments. After measurement of the pristine device, the composite film was switched to the polymer salt and subsequently to the H-bonded state. Cycling tests were performed to test the reversibility of this modification, as shown in Figure 5 and Table 1. It should be noted for calculation of the permeability, it is assumed the scaffold was completely filled and a 2 μm thick LCN top layer was present, see Figure 2A, B. In the pristine state, the gas permeabilities of the composite film for all gasses are low, comparable to other LCN based membranes.[3,29] Although the permeabilities are low, there are still differences in permeability between the individual gasses, being 1.80, 0.05, and 0.46 Barrer for He, N_2, and CO_2, respectively. The differences in permeability are caused by variations in molecular weight, kinetic diameter, critical temperature, and dipole moment.[35] The separation performance of the composite was quantified by calculating the ideal gas selectivity; the greatest selectivity was found for He/N_2 at 35, followed by CO_2/N_2 (9.2) and He/CO_2 (3.9).

To investigate the pH responsive gas permeation, the device was treated with a potassium hydroxide solution to form the reduced order polymer salt composite film as depicted in Figure 2F.[15] The permeation experiments showed that a decrease in polymer order resulted in a large permeation increase for all gasses, with values of 12.55, 7.53, and 6.67 Barrer for He, N_2, and CO_2, respectively, being increase of 1–2 orders of magnitude compared to the pristine and hydrogen-bonded state film. This data also shows, in agreement with the Robeson's

TABLE 1 Gas permeation data of the composite after several switching steps

Sample	Gas	Pristine (Barrer)*	Salt form 1 (Barrer)	H-bonded 1 (Barrer)	Salt form 2 (Barrer)	H-bonded 2 (Barrer)
Composite	He	1.80 ± 0.045	12.55 ± 1.38	1.86 ± 0.11	13.58 ± 0.45	1.37 ± 0.039
Composite	N_2	0.05 ± 0.0043	7.53 ± 0.16	0.56 ± 0.041	7.01 ± 0.28	0.17 ± 0.031
Composite	CO_2	0.47 ± 0.0001	6.67 ± 0.049	0.74 ± 0.022	6.23 ± 0.88	0.36 ± 0.0011
	$*1\,Barrer = 10^{-10}\frac{cm^3_{STP}\cdot cm}{cm^2\cdot s\cdot cmHg}$					

TABLE 2 Gas permeation, solubility coefficient, and diffusivity of the freestanding film

	Permeability			Solubility coefficient CO_2	Diffusivity CO_2
State	He (Barrer)*	N_2 (Barrer)	CO_2 (Barrer)	$\left(\frac{cm^3_{STP}}{cm^3\cdot cmHg}\right)$	$\left(\frac{cm^2}{s}\right)$
Pristine	0.81	0.04	0.12	0.0114	$1.05\cdot 10-9$
Salt form	236.2	114.4	140	0.0259	$5.40\cdot 10-7$
H-bonded	x	x	x	0.0154	x
	$*1\,Barrer = 10^{-10}\frac{cm^3_{STP}\cdot cm}{cm^2\cdot s\cdot cmHg}$				

trade off curve,[36] this increase in permeability is at the expense of selectivity, given that the He/N_2 selectivity decreased from 35 in the pristine state to a value of 1.6 in the salt form.

The system was returned to the H-bonded state by an acidic treatment. Restoring the chemical properties and order in the system also resulted in restoring the gas permeation behavior of the composite film, being again comparable with the pristine state. The repeated reversibility of the system was confirmed by switching between H-bonded and the salt form for two more cycles, in which the gas permeation properties were switched without apparent hysteresis, as depicted in Figure 5.

To investigate the influence of the presence of the scaffold on permeability and permeation of gasses, pure LCN freestanding films with no scaffold were measured. The pristine state of the freestanding films showed permeabilities comparable to the composite film in the pristine state. The freestanding film in the salt form also demonstrated a two orders of magnitude higher permeation rate for all gasses compared to the pristine film, as shown in Table 2. The increase in permeability of the pure LCN film relative to the composite film can be attributed to the greater loss in order when brought into the salt form,[29] as observed during the XRD experiments. Upon switching the freestanding film back to the hydrogen-bonded state, the material restored its mechanical properties but remained physically deformed. This resulted in film fracture, rendering reliable gas permeation experiments impossible. This is in contrast to the composite films that showed sufficient mechanical strength to be handled and repeatedly switched from the basic to the acidic forms allowing repeatable experiments with reproducible results.

As the fabricated membranes can be considered relatively dense, the mechanism of permeation is best described by the solution-diffusion model.[29,37] Here, membranes separate gasses via intrinsic differences in solubility and diffusivity to these gasses. To gain insight in the switchable permeation mechanism, the solubility and diffusivity of CO_2 in the freestanding films was determined. The solubility coefficient of CO_2 approximately doubles when the freestanding film is switched to the salt form, as shown in Table 2. This increase in solubility is attributed to favorable carboxylate salt / CO_2 noncovalent ion-dipole interaction. When switching back to the H-bonded form, the solubility coefficient reduces again, but it does not completely return to the original, pristine state value. There is a $\sim$ 500 fold increase in the diffusivity for the salt form compared to the pristine state, attributed to an increased free volume in the salt form due to the reduced molecular order. These results indicate that the order–disorder transition plays a dominant role in the increase in diffusivity, hence also the leading cause in the increase of permeability of the PP-liquid crystalline composite films.

3 | CONCLUSIONS

A microporous polyolefin film has been functionalized as a composite LCN membrane which can reversibly switch

its gas permeability by more than one order of magnitude via a chemical trigger. The combination of a mechanically rigid, microporous PP scaffold and an LCN brings the best of both worlds together by combining mechanical stability of the former with a dynamic nature with chemical responsiveness of the latter in an easily fabricated device.

This work demonstrates commodity-level polyolefins can be functionalized with nanostructured polymers to create mechanically robust gas separation membranes with switchable permeability properties. New opportunities may lay with in-situ switching for separation of mixtures of gasses and improving detection of gasses with dipole moments including CO, NH_3, CH_3OH, or SO_2.

4 | EXPERIMENTAL SECTION

4.1 | Materials

4-((6-[acryloyloxy]hexyl)oxy)benzoic acid (molecule I) was received from Ambeed Inc. (USA), (4-((4-((6-[acryloyloxy]hexyl)oxy)phenoxy) carbonyl)phenyl 4-((6-[acryloyloxy]hexyl)oxy)benzoate (molecule II) was supplied by Synthon Chemicals. THF and ethanol was purchased from Acros chemicals. Irgacure 819 was supplied by Siba. Celgard2500® was purchased from Celgard®, USA. Polyvinylpyrrolidone (M_w 1.300.000 kg/mol), KOH and HCl was supplied by Sigma-Aldrich.

4.2 | Fabrication composite

Prior to application the glass substrate was cleaned with ultrasonication in a 1:1 mixture of ethanol and acetone and cleaned with UV-Ozone for 30 min in order to increase wettability. A sacrificial layer was applied by spin coating a 5 wt% solution of polyvinylpyrrolidone in ethanol. The LC mixture (Cr 83 SmA 98 N 108 I)., consisting of a 6:4 ratio between molecule I and II, 1 wt% photoinitiator and 0.1 wt% inhibitor was deposited with a thickness of 12 μm onto the sacrificial layer with a wire wound bar coating rod. The sample was heated to 80 °C to the nematic phase at which the scaffold was applied with a pressure roller. After application of the scaffold onto the LC the sample was placed inside a temperature controlled N_2 box in which the sample was cooled from 115 to 85 °C with a cooling rate of 1 °C/min. Subsequently, the sample was polymerized to form a LCN by exposure to an UV-lamp for 15 min with a light intensity of approximately 15 mW/cm^2. The composite was released from the sacrificial layer by immersing the sample in lukewarm water.

4.3 | Fabrication reference samples

Reference samples were made by filling the LC mixture at 110 °C in an anti-parallel rubbed polyimide cell with spacers of 25 μm. After filling of the cells, the samples were given the same heat- and polymerization treatments as the composite films

4.4 | Formation salt form and hydrogen-bonded form

Formation of the salt form was done by submerging the film in a 0.1 M KOH (aq) solution for 30 min. Reforming the hydrogen-bonds was done by submerging the film in a 0.1 M HCl (aq) solution for 30 min. After each switching step FT-IR was used to confirm the conversion.

4.5 | Infra-red spectroscopy

Attenuated total reflection-FT-IR was measured on a Varian 670-IR spectrometer equipped with a golden gate setup.

4.6 | Scanning electron microscopy

SEM analysis was performed on a Quanta FEG 3D SEM in secondary electron mode, with a beam current of 5 kV. Cross-sections of samples were prepared by first submerging the sample into ethanol and freezing of the wetted sample in liquid nitrogen. Subsequently the sample was cut with a scalpel inside the liquid nitrogen parallel to the fibril direction.

4.7 | X-ray scattering

MAXS/WAXS experiments were performed on a Ganesha lab instrument equipped with a Genix-Cu ultralow divergence source producing X-ray photons with a wavelength of 1.54 Å and a flux of 1×10^8 photons per second. Diffraction patterns were collected on a Pilatus 300 K silicon pixel detector with 487×619 pixels of 172 μm^2 with a detector distance of 91 and 500 mm for WAXS and MAXS, respectively.

4.8 | Gas permeation experiments

Single gas permeation experiments were performed using He, N_2, and CO_2 in a stainless-steel cell with membrane area of 2.1 cm^2 with a feed pressure of 6 bar and vacuum at the permeate side. Both freestanding films and composites were supported by an Whatman® filter paper (Grade 50 with pore size of 2.7 μm). Permeabilities were calculated according to Equation 1.

$$P_i = \frac{\Delta P_{permeate} \cdot V_c \cdot V_m \cdot L \cdot 10^{10}}{\Delta t \cdot R \cdot T \cdot A \cdot \Delta P}, \quad (1)$$

with P_i as the permeability of gas i, $\Delta P_{permeate}$ the difference in permeate pressure per time interval Δt, V_c the permeate volume, V_m the molar volume at standard temperature and pressure (STP), L the membrane thickness, R the gas constant, T the temperature in Kelvin, A the membrane area and, ΔP the transmembrane pressure. During each measurement the sample was stabilized over 1 h and subsequently at least three data points were recorded over time. After the three initial gasses, a secondary He permeation experiment proved that the membranes are stable and are insensitive for hysteresis due to CO_2 swelling of the network.

4.9 | Gas sorption experiments

Gas sorption of CO_2 was determined with a Rubotherm series IsoSORP® at 20°C, which uses a magnetically levitating balance to weigh the gas absorbed by the membrane. Helium was used to determine the buoyancy of the membrane, assuming that He is virtually non-soluble in the membrane. By using Equation 2 the corrected mass of was calculated.

$$m_{corrected} = m_{measured} + \rho_{gas} \cdot V_{sample}, \quad (2)$$

in which $m_{corrected}$ was the corrected mass, $m_{measured}$ is the measured mass, ρ_{gas} is the density of the measuring gas and, V_{sample} is the sample volume. Subsequent gas sorption measurements on the sample with either N_2 or CO_2 was performed at 6 bar. By using Equation 3 the concentration gas in the membrane (C_i) was calculated.[29,38]

$$C_i = \frac{m_i \cdot \rho_s}{m_0 \cdot \rho_i\,(STP)}, \quad (3)$$

with ρ_s the density of the membrane and ρ_i(STP) the density of the membrane at STP. By dividing the C_i by the pressure, the eventual solubility was calculated. The corresponding diffusivities were calculated based on Equation 4.

$$D = \frac{P}{S}, \quad (4)$$

in which D is the diffusivity ($\frac{cm^2}{s}$), P is the permeability ($\frac{cm^3_{STP} \cdot cm}{cm^2 \cdot s \cdot cmHg}$) and S is the solubility coefficient ($\frac{cm^3_{STP}}{cm^3 \cdot cmHg}$).

ACKNOWLEDGMENTS

Authors would like to thank S.S.D. Lugger for performing the XRD measurements and M. Houben for valuable discussions. Authors would also like to thank Prof. dr. D.-J. Broer and dr. M.G. Debije for critically reviewing this manuscript. Data available within the article.

ORCID

Simon J. A. Houben https://orcid.org/0000-0002-9158-056X
Joey Kloos https://orcid.org/0000-0002-7821-7256
Zandrie Borneman https://orcid.org/0000-0003-2215-8987
Albert P. H. J. Schenning https://orcid.org/0000-0002-3485-1984

REFERENCES

[1] X. Feng, M. E. Tousley, M. G. Cowan, B. R. Wiesenauer, S. Nejati, Y. Choo, R. D. Noble, M. Elimelech, D. L. Gin, C. O. Osuji, *ACS Nano* **2014**, *8*(12), 11977.
[2] H. Katayama, T. Kato, K. Hamaguchi, D. Kuo, M. Liu, T. Sakamoto, M. Yoshio, H. Katayama, T. Kato, *ACS Macro Lett.* **2019**, *8*(1), 24.
[3] J. E. Bara, A. K. Kaminski, R. D. Noble, D. L. Gin, *J. Memb. Sci.* **2007**, *288*, 13.
[4] K. K. Mokwena, J. Tang, *Crit. Rev. Food Sci. Nutr.* **2012**, *52*(7), 640.
[5] D. L. Gin, J. E. Bara, R. D. Noble, B. J. Elliott, *Macromol. Rapid Commun.* **2008**, *29*, 367.
[6] S. Basu, A. L. Khan, A. Cano-Odena, C. Liu, I. F. J. Vankelecom, *Chem. Soc. Rev.* **2010**, *39*(2), 750.
[7] R. W. Baker, K. Lokhandwala, *Ind. Eng. Chem. Res.* **2008**, *47*(7), 2109.
[8] E. P. A. V. Heeswijk, J. J. H. Kloos, J. D. Heer, T. Hoeks, N. Grossiord, A. P. H. J. Schenning, *ACS Appl. Mater. Interfaces* **2018**, *10*(35), 30008.
[9] A. J. J. Kragt, D. C. Hoekstra, S. Stallinga, D. J. Broer, A. P. H. J. Schenning, *Adv. Mater.* **2019**, *31*, 1.
[10] M. Pilz da Cunha, Y. Foelen, R. J. H. van Raak, J. N. Murphy, T. A. P. Engels, M. G. Debije, A. P. H. J. Schenning, *Adv. Opt. Mater.* **2019**, *7*(7), 1801643.
[11] R. C. P. Verpaalen, S. Varghese, A. Froyen, M. Pilz da Cunha, M. J. Pouderoijen, J. R. Severn, M. R. Bhatti, T. Peijs, C. W. M. Bastiaansen, M. G. Debije, et al., *Matter* **2020**, *2*(6), 1522.
[12] J. A. M. Lugger, P. P. M. S. Román, C. C. E. Kroonen, R. P. Sijbesma, *ACS Appl. Mater. Interfaces* **2021**, *13*, 4385.

[13] J. D. Willott, W. M. Nielen, W. M. De Vos, *ACS Appl. Polym. Mater.* **2020**, *2*, 659.
[14] Y. Wang, Z. Liu, B. Han, Z. Dong, J. Wang, D. Sun, Y. Huang, G. Chen, *Polymer* **2004**, *45*, 855.
[15] S. J. A. Houben, S. A. van Merwijk, B. J. H. Langers, B. M. Oosterlaken, Z. Borneman, A. P. H. J. Schenning, *ACS Appl. Mater. Interfaces* **2021**, *13*(6), 7592.
[16] M. Moirangthem, R. Arts, M. Merkx, A. P. H. J. Schenning, *Adv. Funct. Mater.* **2016**, *26*, 1154.
[17] Y. Foelen, D. A. C. Van Der Heijden, M. Del Pozo, J. Lub, C. W. M. Bastiaansen, A. P. H. J. Schenning, *ACS Appl. Mater. Interfaces* **2020**, *12*(14), 16896.
[18] R. C. P. Verpaalen, M. Pilz da Cunha, T. A. P. Engels, M. G. Debije, A. P. H. J. Schenning, *Angew. Chemie - Int. Ed.* **2020**, *59*(11), 4532.
[19] G. H. Timmermans, R. F. Douma, J. Lin, M. G. Debije, *Appl. Sci.* **2020**, *10*(4), 1–9.
[20] A. Ryabchun, F. Lancia, A. D. Nguindjel, N. Katsonis, *Soft Matter* **2017**, *13*(44), 8070.
[21] G. Kocak, C. Tuncer, V. Bütün, *Polym. Chem.* **2017**, *8*(1), 144.
[22] A. Cao, R. J. H. Van Raak, D. J. Broer, *Soft Matter* **2019**, *15*(23), 4737.
[23] D. Wandera, S. R. Wickramasinghe, S. M. Husson, *J. Memb. Sci.* **2010**, *357*(1–2), 6.
[24] A. Cao, R. J. H. V. Raak, X. Pan, D. J. Broer, *Adv. Funct. Mater.* **2019**, *1900857*(378), 1.
[25] X. Lu, S. Guo, X. Tong, H. Xia, Y. Zhao, *Adv. Mater.* **2017**, *29*(28), 1.
[26] L. Gao, G. Guo, M. Liu, Z. Tang, L. Xie, Y. Huo, *RSC Adv.* **2017**, *7*(63), 40005.
[27] J. Shang, S. Lin, P. Theato, *Polym. Chem.* **2018**, *9*(23), 3232.
[28] S. S. D. Lafleur, J. R. Severn, R. C. P. Verpaalen, A. P. H. J. Schenning, C. W. M. Bastiaansen, *ACS Appl. Polym. Mater.* **2019**, *1*(3), 392.
[29] J. Kloos, N. Jansen, M. Houben, A. Casimiro, J. Lub, Z. Borneman, A. P. H. J. Schenning, K. Nijmeijer, *Chem. Mater* **2021**, *33*, 8323.
[30] C. L. Gonzalez, C. W. M. Bastiaansen, J. Lub, J. Loos, K. Lu, H. J. Wondergem, D. J. Broer, *Adv. Mater.* **2008**, *20*, 1246.
[31] A. Longo, D. J. Mulder, H. P. C. Van Kuringen, D. Hermida-Merino, D. Banerjee, D. Dasgupta, I. K. Shishmanova, A. B. Spoelstra, D. J. Broer, A. P. H. J. Schenning, et al., *Chem. - A Eur. J.* **2017**, *23*(51), 12534.
[32] H. P. C. Van Kuringen, G. M. Eikelboom, I. K. Shishmanova, D. J. Broer, A. P. H. J. Schenning, *Adv. Funct. Mater.* **2014**, *24*, 5045.
[33] I. K. Shishmanova, C. W. M. Bastiaansen, A. P. H. J. Schenning, D. J. Broer, *Chem. Commun.* **2012**, *48*(38), 4555.
[34] H. P. C. van Kuringen, *Eindhoven Univer. Techol.* **2016**.
[35] R. A. M. Hikmet, J. Lub, A. J. W. Tol, *Macromolecules* **1995**, *28*(9), 3313.
[36] L. M. Robeson, *J. Memb. Sci.* **1991**, *62*, 165.
[37] S. C. George, S. Thomas, *Prog. Polym. Sci.* **2001**, *26*, 985.
[38] S. He, X. Jiang, S. Li, F. Ran, J. Long, L. Shao, *AIChE J.* **2020**, *66*(10), 1.

How to cite this article: S. J. A. Houben, J. Kloos, Z. Borneman, A. P. H. J. Schenning, *J. Polym. Sci.* **2022**, *60*(5), 803. https://doi.org/10.1002/pol.20210835